DOI: 10.1002/cphc.201100456

Two-Photon STED Spectral Determination for a New V-Shaped Organic Fluorescent Probe with Efficient Two-Photon Absorption

Kevin D. Belfield,*[a, b] Mykhailo V. Bondar,[c] Alma R. Morales,[a] Lazaro A. Padilha,[b] Olga V. Przhonska,[c] and Xuhua Wang[a]

Dedicated to the memory of William von Eggers Doering

Two-photon stimulated emission depletion (STED) cross sections were determined over a broad spectral range for a novel two-photon absorbing organic molecule, representing the first such report. The synthesis, comprehensive linear photophysical, two-photon absorption (2PA), and stimulated emission properties of a new fluorene-based compound, (*E*)-2-{3-[2-(7-(diphenylamino)-9,9-diethyl-9H-fluoren-2-yl)vinyl]-5-methyl-4-oxocyclohexa-2,5-dienylidene} malononitrile (**1**), are presented. Linear spectral parameters, including excitation anisotropy and fluorescence lifetimes, were obtained over a broad range of organic solvents at room temperature. The degenerate two-photon absorption (2PA) spectrum of **1** was determined with a combination of the direct open-aperture Z-scan and relative two-photon-induced fluorescence methods using 1 kHz femtosecond excitation. The maximum value of the 2PA cross section ~1700 GM was observed in the main, long wavelength, one-photon absorption band. One- and two-photon stimulated emission spectra of **1** were obtained over a broad spectral range using a femtosecond pump–probe technique, resulting in relatively high two-photon stimulated emission depletion cross sections (~1200 GM). A potential application of **1** in bioimaging was demonstrated through one- and two-photon fluorescence microscopy images of HCT 116 cells incubated with micelle-encapsulated dye.

1. Introduction

The processes of one- and two-photon stimulated electronic transitions in organic molecules are of increasing scientific and technological interest due to their potential nonlinear optical applications in two-photon induced fluorescence microscopy (2PFM),[1–4] high-density 3D optical data storage and microfabrication,[5–8] one- and two-photon optical power limiting,[9,10] high-resolution molecular spectroscopy,[11] and optical switching and light amplification of stimulated emission.[12–14] The nature of different types of stimulated transitions determines specific peculiarities in structure–property relationships that should be considered in a variety of nonlinear optical measurements. The investigation of two-photon stimulated emission transitions is intriguing and was reported, primarily for atomic systems.[15,16] In the case of organic molecular structures, this phenomenon was reported for the first time for a sulfonyl-containing fluorene derivative[17] which also exhibited efficient two-photon absorption (2PA) and lasing properties.[18] The technique for two-photon-stimulated emission measurements, until now, is not well-developed, in contrast to the known and widespread 2PA methodologies.[19,20] One of the promising methods for the investigation of the excited-state molecular dynamics, including stimulated emission transitions that occur in organic molecules, is a fluorescence quenching methodology described by Lakowicz.[21–23] This technique allows modification of the molecular orientational distribution in the excited states,[24,25] creates anisotropic molecular ensembles with specific fluorescence properties,[23] and can reveal the values of one- and two-photon stimulated emission cross sections.[17] The determination of the spectral dependences of one- and two-photon stimulated emission cross sections in combination with comprehensive 2PA investigations is important for further development of high-resolution two-photon fluorescence imaging[26,27] and, in particular, for stimulated emission depletion (STED) microscopy.[1,28,29]

Herein, we report the comprehensive linear photophysical, 2PA, and stimulated emission properties of (*E*)-2-{3-[2-(7-(diphenylamino)-9,9-diethyl-9H-fluoren-2-yl)vinyl]-5-methyl-4-oxocyclohexa-2,5-dienylidene} malononitrile (**1**), a new V-shaped fluorene derivative, in a broad range of organic solvents at room temperature. The values of 2PA and stimulated emission cross sections of **1** were obtained using 1 kHz tunable femtosecond laser systems by open-aperture Z-scan as well as two-photon induced fluorescence (2PF) methods[19,20] and a pump–probe

[a] *Prof. K. D. Belfield, Dr. A. R. Morales, X. Wang*
Department of Chemistry
University of Central Florida
P.O. Box 162366, Orlando, FL 32816-2366 (USA)
E-mail: belfield@ucf.edu

[b] *Prof. K. D. Belfield, Dr. L. A. Padilha*
CREOL, The College of Optics and Photonics
University of Central Florida
P.O. Box 162366, Orlando, FL 32816-2366 (USA)

[c] *Dr. M. V. Bondar, Dr. O. V. Przhonska*
Institute of Physics National Academy of Sciences of Ukraine
Prospect Nauki, 46, Kiev-28, 03028 (Ukraine)

fluorescence quenching technique,[17] respectively. The potential of **1** for use in bioimaging was demonstrated through one- and two-photon fluorescence microscopy of epithelial colorectal carcinoma HCT 116 cells incubated with probe **1** encapsulated in Pluronic F 108 NF micelles.

2. Results and Discussion

2.1. Linear Spectral Properties of 1

The method for preparing the symmetrical chromophore **1** is outlined in Scheme 1. Chromophore **1** is a class of red dye containing a 2-pyran-4-ylidenemalononitrile as an electron acceptor moiety and diphenylamine as electron donor. The two

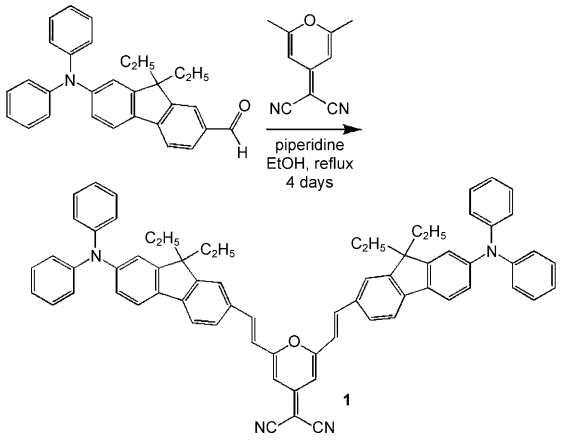

Scheme 1. Synthesis of fluorenyl-probe **1**.

cyano groups of 2-pyran-4-ylidenemalononitrile are electron-withdrawing groups and the electron-deficient pyran ring can act as auxiliary acceptor. The chromophore was prepared through Knoevenagel condensation between 2-(2,6- dimethypyran-4-ylidene) malononitrile and the 7-(diphenylamino)-9,9-diethyl-9H-fluorene-2-carbaldehyde (**A**). In the condensation reaction both mono and di-reaction takes places, resulting in the linear and V-shaped compounds, respectively. These were readily separated by column chromatography. The molecular structure of **1** was confirmed by ^{1}H and ^{13}C NMR, and high-resolution mass spectra (HRMS). This compound readily dissolves in common solvents, such as cyclohexane (CHX), toluene (TOL), chloroform ($CHCl_3$), *ortho*-dichlorobenzene (ODCB), tetrahydrofuran (THF), polytetrahydrofuran (pTHF), dichloromethane (CH_2Cl_2) and acetonitrile (ACN).

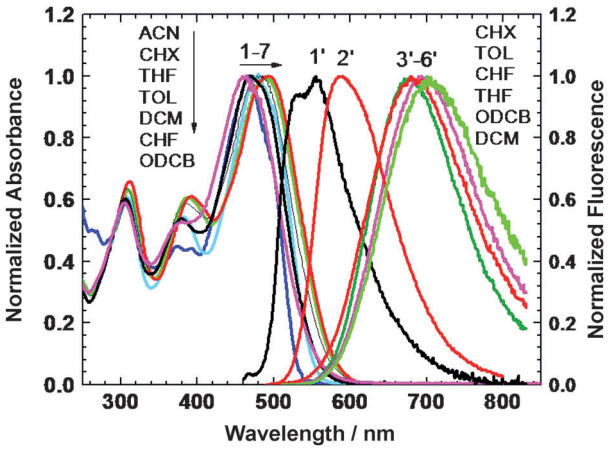

Figure 1. Normalized steady-state absorption (1–7) and fluorescence (1′–6′) spectra of **1** in ACN (1), CHX (2, 1′), TOL (4, 2′), CHCl3 (6, 3′), THF (3, 4′), ODCB (7, 5′) and CH2Cl2 (5, 6′).

The steady-state absorption and fluorescence spectra along with the main photophysical parameters of **1** are presented in Figure 1 and Table 1. In contrast to linear symmetrical fluorenes,[18,30] the structure of **1** possesses a relatively large "*y*" component of the stationary dipole moment resulting in the complicated behavior of λ_{abs}^{max} and weak spectral shifts of ≈20–30 nm in solvents of differing polarity Δf (Figure 1, curves 1–7). The steady-state fluorescence spectra of **1** (curves 1′–6′) exhibit strong solvatochromic effects with Stokes shifts of up to ≈290 nm in polar ACN (see Table 1), while good correspondence to the Lippert equation[31] is observed (Figure 2a). This is consistent with a large change in the stationary dipole moment occurring under electronic excitation $S_0 \rightarrow S_1$ and a dominant role of general solute–solvent interactions. Fluorescence quantum yields, Φ, and lifetimes, τ, of **1** exhibit relatively complex dependences on solvent polarity, Δf (see Table 1), which can be roughly explained by the combination of the Onsager and Bohr models for general solute–solvent interactions, as already reported.[32,33]

Table 1. Main photophysical parameters of **1** in solvents with different polarity Δf and viscosity η: absorption λ_{abs}^{max} and fluorescence λ_{fl}^{max} maxima, Stokes shifts, maximum extinction coefficients ε^{max}, quantum yields Φ and fluorescence lifetimes, τ.

N/N	CHX	TOL	$CHCl_3$	ODCB	THF	CH_2Cl_2	ACN
Δf[a]	3×10^{-4}	0.014	0.148	0.186	0.209	0.217	0.305
η [cP]	0.97	0.59	0.54	1.32	0.48	0.4	0.34
λ_{abs}^{max} [nm]	467 ± 1	477 ± 1	488 ± 1	492 ± 1	469 ± 1	480 ± 1	463 ± 1
λ_{fl}^{max} [nm]	555 ± 1	589 ± 1	678 ± 1	694 ± 1	682 ± 1	704 ± 1	755 ± 5
Stokes shift	3430 ± 100	3990 ± 100	5740 ± 100	5920 ± 100	6660 ± 100	6630 ± 100	8350 ± 100
[cm^{-1}] [nm]	(88 ± 2)	(112 ± 2)	(190 ± 2)	(202 ± 2)	(213 ± 2)	(224 ± 2)	(292 ± 6)
ε^{max} x10^{-3} [$M^{-1}cm^{-1}$]	–	76 ± 4	70 ± 4	69 ± 4	73 ± 4	71 ± 4	–
$\Phi\times10^{2}$	2.7 ± 0.5	20 ± 2	32 ± 3	20 ± 2	13 ± 2	5.7 ± 1	0.2 ± 0.1
τ [ns]	0.2 ± 0.08	0.95 ± 0.08	2.4 ± 0.08	1.85 ± 0.08	1.38 ± 0.08	0.63 75 % 2.6 25 %	–

[a] Orientation polarizability $\Delta f = (\varepsilon - 1)/(2\varepsilon + 1) - (n^2 - 1)/(2n^2 + 1)$ (ε and n are the dielectric constant and refraction index of the medium, respectively).[31]

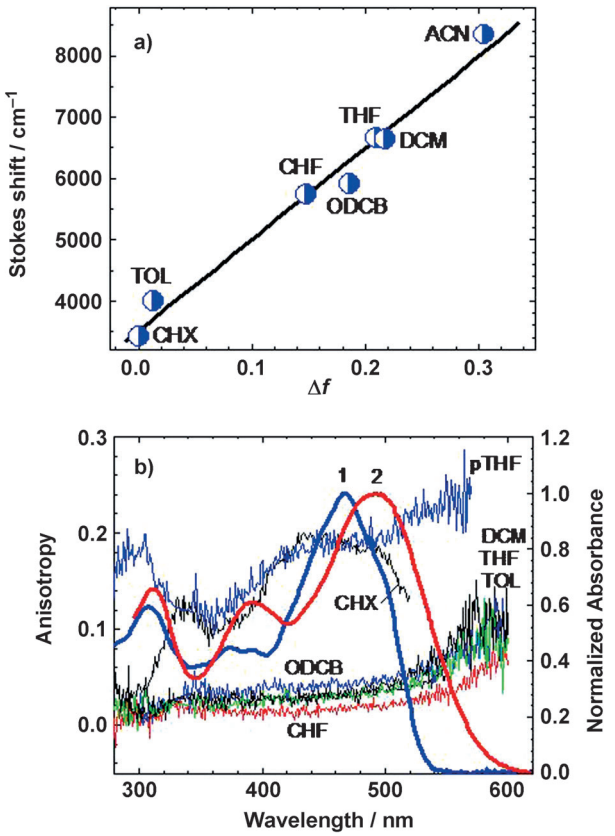

Figure 2. a) Lippert plot for **1**. b) Excitation anisotropy spectra of **1** in pTHF, CHX, ODCB, CH_2Cl_2, THF, TOL, $CHCl_3$ and normalized absorbance in CHX (1) and ODCB (2).

All fluorescence decay processes revealed a single-exponential profile, except for the CH_2Cl_2 solution of **1**. The highest values of Φ and τ were observed in $CHCl_3$, and therefore this solvent was the most appropriate for stimulated emission measurements and 2PA investigations by the 2PF method. The excitation anisotropy spectrum of **1** in viscous pTHF (Figure 2b) revealed relatively low fundamental values $r_0(\lambda_{ex}) \approx 0.18$–$0.24$ in the spectral range $420 < \lambda_{ex} < 570$ nm, indicative of the complicated electronic structure of the main long-wavelength absorption band and including at least two singlet–singlet transitions. The shapes of excitation anisotropy spectra in low-viscosity solvents are sufficiently close to each other (Figure 2b, CH_2Cl_2, THF, TOL, $CHCl_3$) with corresponding absolute values of r depending on the ratio τ/θ [see Eq. (2)]. Similar shapes of the excitation anisotropy spectra $r(\lambda_{ex})$ is evidence for the similar space orientation of the corresponding transition dipoles $S_0 \rightarrow S_n$ ($n = 1, 2, 3, \ldots$). The calculated electronic spectrum of **1** along with the steady-state absorption spectrum in CHX is presented in Figure 3. From these calculations, one can conclude that the main long-wavelength absorption band is determined by two close electronic transitions $S_0 \rightarrow S_1$ (HOMO−1→LUMO) and $S_0 \rightarrow S_2$ (HOMO→LUMO) with comparable oscillator strengths (1.20 and 1.66, respectively) and different space orientation (the angle between corresponding transition dipoles $\alpha \approx 90^\circ$). A large value of α explains the sufficiently low excitation anisotropy $r_0(\lambda_{ex})$ which was observed in

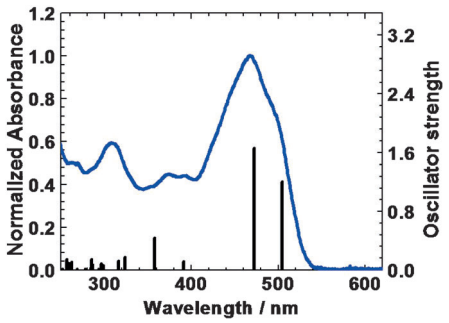

Figure 3. Calculated electronic spectrum of **1** in vacuum (vertical black lines, value of each corresponds to the oscillator strength) and normalized absorption spectrum of **1** in CHX (blue).

the main absorption band (Figure 2b, pTHF) in contrast to linear symmetrical fluorenes.[18,30] Taking into account relatively small changes in the fundamental values $r_0(\lambda_{ex}) \approx 0.18$–$0.24$, the range of corresponding angles between absorption $S_0 \rightarrow S_1$ and emission $S_1 \rightarrow S_0$ transition dipoles can be estimated as 30–40°. The calculated change in the stationary dipole moment of **1** under electronic excitation (≈6 D) was consistent with the strong solvatochromic behavior of the observed fluorescence spectra.

2.2. 2PA spectra of 1

The efficiency of degenerate 2PA processes in a $CHCl_3$ solution of **1** (Figure 4, curves 1, 1′) was investigated over a broad spectral range by the combination of open-aperture *Z*-scan and 2PF methods.[19,20] The short-wavelength portion of the 2PA spectrum ($650 < \lambda_{ex} < 820$ nm) was obtained by *Z*-scan, and the long-wavelength sections ($760 < \lambda_{ex} < 1170$ nm) by the second, more sensitive method (2PF), respectively. In the overlapping spectral range ($760 < \lambda_{ex} < 820$ nm) good agreement between these two independent data sets is observed. According to Figure 4 (curves 1, 1′), fluorenyl **1** exhibited two well-defined

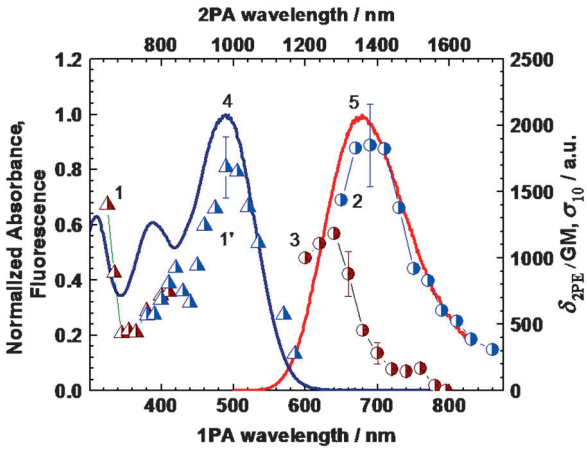

Figure 4. Spectroscopic data of **1** in $CHCl_3$: 2PA spectrum obtained by open-aperture *Z*-scan (1) and 2PF (1′) methods; one- (2) and two-photon (3) stimulated emission spectra; normalized steady-state absorption (4) and fluorescence (5) spectra.

2PA bands with a maximum 2PA cross section, $\delta_{2PA} \approx 1700$ GM, at the corresponding one-photon absorption (1PA) maximum of the main long-wavelength band. The beginning of a third peak is observed for photon energies near the low-energy 1PA edge, but the peak position cannot be determined due to the tail of the linear absorption spectrum. The spectral position of the most intense 2PA band is not typical for symmetrical fluorenes (as a rule, a monotonic decrease in the region of linear absorption band is observed[18,34]) and can be ascribed to the complicated electronic nature of the main long-wavelength 1PA band of **1** described above. The second, less intense 2PA maximum, $\delta_{2PA} \approx 900$ GM at $\lambda_{ex} \approx 840$ nm, can be attributed to a one-photon forbidden electronic transition revealed from the quantum chemical calculations. To assess the photostability of **1**, its photochemical decomposition quantum yield was determined in THF upon excitation in the main absorption band and is $\Phi_{Ph} \approx 4 \times 10^{-7}$. The corresponding characteristic parameter by which all 2PA fluorescent probes can be compared (the figure of merit)[35] is $F_M = (\delta_{2PA}\Phi)/\Phi_{Ph} \approx 5 \times 10^8$ GM. For comparison, Fluorescein in water (pH 11) exhibits $F_M \approx 6 \times 10^6$ GM under the same experimental conditions. The new V-shaped probe possesses a F_M of approximately two orders of magnitude greater than Fluorescein, a widely used fluorescent probe. The relatively high values of the δ_{2PA} (~500–1700 GM), at wavelengths that fall nicely within the tuning range of the Ti:sapphire laser, coupled with the high F_M, strongly suggest the potential of **1** for 2PFM bioimaging.

2.3. One- and Two-Photon Stimulated Emission Spectra

The spectral dependences of the one- and two-photon stimulated emission cross sections $\sigma_{10}(\lambda_q)$ and $\delta_{2PE}(\lambda_q)$, respectively, were obtained over a broad spectral range (Figure 4, curves 2,3) by a pump–probe fluorescence quenching method described in detail previously.[17] The linear dependences $1 - I_F/I_{F0} \sim \sigma_{10}(\lambda_q)^q E_P$ and $1 - I_F/I_{F0} \sim \delta_{2PE}(\lambda_q)^q E_P^2$ were observed for each excitation wavelength (Figure 5, see Experimental Section for details). These dependences exhibit the nature of one- and two-photon STED processes. Furthermore, the combination of the spectral independence of the fluorescence quantum yield and high photostability of **1** strongly supports one- and two-photon stimulated emission transitions. According to Figure 4 (curve 2), the shape and absolute values of the one-photon stimulated emission contour $\sigma_{10}(\lambda_q)$ (curve 2) are sufficiently close to the steady-state fluorescence spectrum (curve 5) with only a small long-wavelength shift (~15 nm), in accordance with the theoretical prediction for the spectral dependence of $\sigma_{10} \sim \lambda^4 \cdot I_F(\lambda)$.[36] This behavior is consistent with the observed solvatochromic properties of **1**, confirming a dominant role of the general solvent–solute effects in $CHCl_3$. The two-photon stimulated emission spectrum $\delta_{2PE}(\lambda_q)$ (curve 3) is shifted to a shorter wavelength (relative to curves 2, 5), exhibiting a maximum at $\lambda_q/2 \approx 640$ nm with a corresponding cross section of about 1200 GM. The delay time between the pump and quenching pulses is ≈10 ps, which appears sufficient for completion of all solvent relaxation processes in the S_1 state.[31] It may be assumed that the maximum of

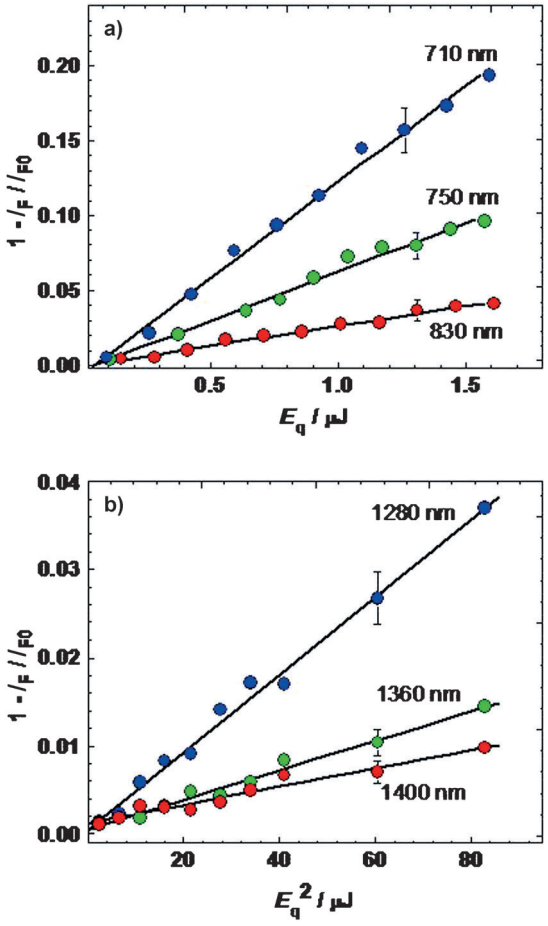

Figure 5. Dependences $1 - I_F/I_{F0} = f(^qE_P)$ and $1 - I_F/I_{F0} = f(^qE_P^2)$ for fluorescence quenching of **1** in $CHCl_3$. a) One-photon STED at 710 nm (blue circles), 750 nm (green circles), and 830 nm (red circles). b) Two-photon STED at 1280 nm (blue circles), 1360 nm (green circles), and 1400 nm (red circles). The solid black lines are linear fittings.

δ_{2PE} should be close to the observed fluorescence peak at ≈680 nm in the case when the nature of two-photon stimulated emission $S_1 \rightarrow S_0$ is similar to the corresponding 2PA $S_0 \rightarrow S_1$ process.[37] In contrast to this assumption, a short wavelength shift of the δ_{2PE} maximum was observed, suggesting that further theoretical and experimental investigations are needed to gain a deeper understanding of this phenomenon.

2.4. One- and Two-Photon Bioimaging

Cell imaging under one- and two-photon fluorescence excitation was performed to demonstrate the potential utility of **1** in 2PFM bioimaging. Pluronic F 108 NF micelles were employed to encapsulate the hydrophobic probe **1** for incubation with epithelial colorectal carcinoma HCT 116 cells. 1PFM and 2PFM images of the probe-incubated cells are shown in Figure 6, clearly indicating that the micelle-encapsulated probe is readily taken up by the cells. 2PFM images of the cell correspond well with 1PFM images but with higher contrast. In the 2PFM images, the nucleus of the cell is evident and the organelles

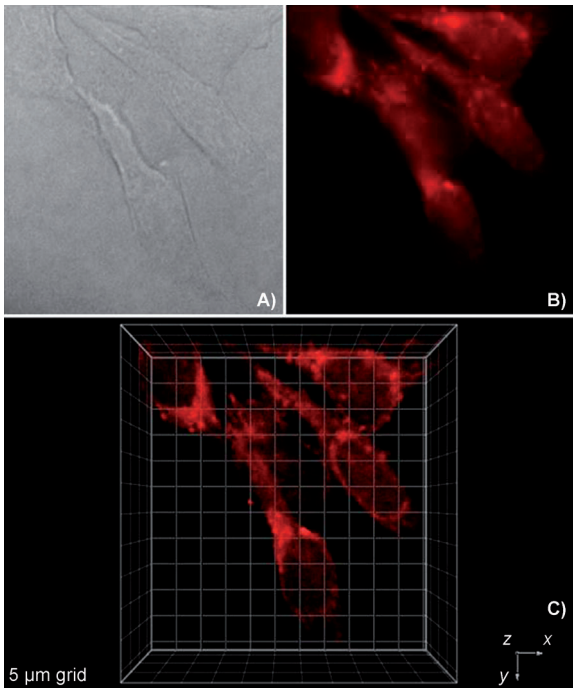

Figure 6. Images of HCT 116 cells incubated with micelle-encapsulated **1** (50 μM, 2 h). A) DIC, B) one-photon fluorescence microscopy image, C) 3D reconstruction from overlaid two-photon fluorescence microscopy images (Ex: 940 nm; power: 120 mW; Em. short-pass filter 800 nm); 5 μm grid.

can be seen clearly. The organelles in which the probe localizes are likely lysosomes, as we previously demonstrated.[38,39]

3. Conclusions

A new, V-shaped fluorenyl probe **1** was synthesized and comprehensively characterized in a variety of organic solvents of differing polarity at room temperature. Strong solvatochromic effects for this V-shaped symmetrical molecule corresponded to the Lippert equation, indicative of the dominant role of general solute–solvent interactions. Quantum chemical calculations along with excitation anisotropy spectra of **1** revealed the rather complex nature of the main 1PA band, primarily due to two noncolinear electronic transitions with comparable oscillator strengths. The values of lifetimes and fluorescence quantum yields of **1** exhibit somewhat complicated dependences on solvent polarity. The degenerate 2PA spectrum of symmetrical compound **1** exhibited two well-defined bands with a maximum cross section of ≈1700 GM at the corresponding 1PA maximum of the main long-wavelength band.

Quite significantly, this work is the first report of quantitative two-photon stimulated emission properties over a broad spectral range for an organic compound. One- and two-photon stimulated emission spectra of **1** were obtained over a broad spectral region by a fluorescence-quenching femtosecond pump–probe technique. The one-photon STED spectrum closely overlaps the steady-state fluorescence emission spectrum. The two-photon STED spectrum exhibits a maximum cross section of ≈1200 GM and is shifted to shorter wavelengths by about 60 nm relative to the one-photon STED spectrum. This behavior is not fully understood and may be a subject of further investigation. The high figure of merit of probe **1** provides compelling support for its use in bioimaging. This was demonstrated through one- and two-photon laser scanning fluorescence microscopy of epithelial colorectal carcinoma HCT 116 cells that were incubated with Pluronic F 108 NF micelle-encapsulated **1**, showing lysosomal localization. The high 2PA, F_M, and stimulated emission efficiencies of the new fluorene-based probe **1** make it a promising candidate for 2PFM and STED imaging, both aspects of future investigation.

Experimental Section

Materials and Synthetic Procedures: Chemicals were purchased from either Aldrich or Acros Chemical Co. and used as received. Piperidine was dried over CaH_2, distilled under reduced pressure, and stored over 4 Å molecular sieves. 7-(Diphenylamino)-9,9-diethyl-9*H*-fluorene-2-carbaldehyde (A) was synthesized according to a published procedure.[40]

Synthesis of (E)-2-{3-[2-(7-(diphenylamino)-9,9-diethyl-9H-fluoren-2-yl)vinyl]-5-methyl-4-oxocyclohexa-2,5-dienylidene} malononitrile (**1**): A mixture of 7-(diphenylamino)-9,9-diethyl-9*H*-fluorene-2-carbaldehyde (**A**) (0.6 g, 1.43 mmol), and commercial 2,6-dimethyl-4-dicyanomethylene-4H-pyran (0.13 g, 0.71 mmol) were dissolved in EtOH (35 mL). After adding piperidine (0.4 mL) slowly via syringe while stirring, the reaction mixture was refluxed for 72 h. A reddish precipitate was obtained after cooling the reaction to room temperature. Compound **1** was obtained after purifying the product through a silica gel column using hexanes/ethyl acetate (4:1) as eluent. A red solid was obtained (0.35 g, 25% yd); m.p. 229–230 °C. ^{1}H NMR (300 MHz, $CDCl_3$) $\delta = 7.68$ (s, 1H), 7.66 (s, 2H), 7.60–7.52 (m, 8H), 7.30–7.24 (m, 10H), 7.15–7.10 (m, 10H), 7.06–7.01 (m, 5H) 6.84 (s, 1H), 6.79 (s, 1H), 6.72 (s, 2H), 2.01–1.94 (m, 8H), 0.39 ppm (t, $J = 14.7$ Hz, 12H). ^{13}C NMR (75 MHz, $CDCl_3$) $\delta = 158.6$, 155.8, 152.0, 150.8, 148.2, 147.7, 144.2, 138.6, 135.1, 132.5, 129.2, 127.8, 124.2, 1232.2, 122.9, 121.6, 121.0, 119.5, 118.6, 117.1, 115.4, 106.8, 59.0, 56.1, 32.6, 8.6 ppm. HRMS-ESI theoretical m/z $[M+H]^+ =$ 971.47, found, 971.46, theoretical; m/z $[2M+H]^+ = 1941.93$, found, 1941.92, theoretical.

Linear Photophysical Measurements and Computational Details: The linear one-photon absorption (1PA), fluorescence, and excitation anisotropy spectra of **1** were investigated in spectroscopic grade CHX, TOL, $CHCl_3$, ODCB, THF, CH_2Cl_2 and ACN at room temperature. The steady-state absorption spectra were obtained with an Agilent 8453 UV/Vis spectrophotometer in 10 mm path length quartz cuvettes with dye concentrations $C \sim 10^{-5}$ M. The steady-state fluorescence emission and excitation anisotropy spectra were measured with a PTI QuantaMaster spectrofluorimeter in 10 mm spectrofluorometric quartz cuvettes with $C \sim 10^{-6}$ M. All fluorescence spectra were corrected for the spectral responsivity of the PTI detection system. Excitation anisotropy measurements were performed in "L-format" configuration[31] with viscous pTHF used as solvent for the determination of the fundamental anisotropy values of **1** [Eq. (1)]:

$$r_0 = (3\cos^2\alpha - 1)/5 \quad (1)$$

where α is the angle between absorption $S_0 \rightarrow S_1$ and emission $S_1 \rightarrow S_0$ transition dipoles (S_0 and S_1 are the ground and first excited molecular electronic state, respectively). In pTHF, the value of rota-

tional correlation time, $\theta \gg \tau$ (τ is the molecular fluorescence lifetime) and the experimentally observed anisotropy was close to the fundamental value [Eq. (2)]:[41]

$$r = r_0/(1+\tau/\theta) \approx r_0 \qquad (2)$$

Fluorescence lifetimes of **1**, τ, were measured with a single-photon counting system, PicoHarp 300, with time resolution of ≈80 ps under the excitation of linearly polarized and oriented by the magic angle femtosecond laser beam (MIRA 900, Coherent). The values of fluorescence quantum yields of **1**, Φ, were obtained by a relative method using 9, 10-diphenylanthracene in CHX as the standard.[42] The photochemical decomposition quantum yield of **1**, Φ_{Ph}, was determined in THF under one-photon excitation (Loctite-97034 UV lamp) by the previously described absorption method.[43] An additional analysis of the electronic structure of **1** was performed by semi-empirical quantum chemical calculations using HyperChem V7.0 for Windows. The optimized ground-state geometry was obtained using AM1 approximation. The procedure for optimization was stopped upon reaching a gradient of 0.01 kcal mol^{-1}. Electronic spectra of **1** in vacuum were determined by the ZINDO/S method with the ten highest occupied molecular orbitals (HOMOs) and the ten lowest unoccupied molecular orbitals (LUMOs). Average overlap weighting factors of 1.267 and 0.49 were used for σ and π bonds, respectively. The value of the π weighting factor was chosen to obtain acceptable agreement between the energies of the calculated and experimentally observed long-wavelength $S_0 \rightarrow S_1$ electronic transition. It should be mentioned that the changes in the π weighting factor in the range of 0.46–0.52 did not significantly alter the relative positions of the electronic levels.

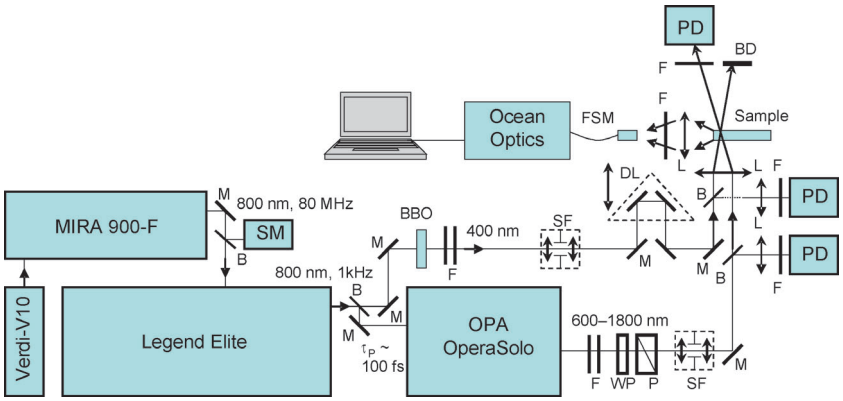

Figure 7. Experimental setup. M: 100% reflection mirrors, B: beam splitters, SM: spectrometer, BBO: 1 mm crystal, F: set of neutral and/or interferometric filters, SF: space filters, WP: wave plate $\lambda/2$, P: polarizer, DL: optical delay line with retro-reflector; Sample: 1 mm quartz cuvette containing sample, FSM: fiber optic spectrometer HR4000, PD: calibrated Si and/or InGaAs photodetectors, L: focusing lenses, BD: beam dump.

2PA Measurements: The degenerate 2PA spectra of **1** were measured in $CHCl_3$ over a broad spectral region by open-aperture *Z*-scan[19] and relative two-photon (2PF) methods[20] with Rhodamine B in methanol and Fluorescein in water (pH 11) as standards.[44] Two-photon induced fluorescence spectra were obtained with a PTI QuantaMaster spectrofluorimeter coupled with a femtosecond Clark-MXR CPA-2010 laser with pumped optical parametric generator/amplifiers (TOPAS), generating ≈140 fs output pulses (FWHM) with repetition rate of 1 kHz. The quadratic dependence of 2PF intensity on the excitation power was confirmed for each excitation wavelength, λ_{ex}. The same laser system was used for open-aperture *Z*-scan measurements. The open-aperture *Z*-scan calibration was verified with ZnSe and CdTe, which are 2PA standards. A comprehensive description of this experimental methodology was previously reported.[45,46]

One- and Two-Photon Stimulated Emission Cross Section Measurements: The investigation of stimulated emission transitions in **1** were performed based on pump–probe fluorescence quenching methodology[17] using the femtosecond laser system (Coherent, Inc.), depicted in Figure 7. The output of a 76 MHz Ti:sapphire laser (Mira900-F tuned to 800 nm, with average power ≈1.1 W and pulse duration 200 fs), pumped by the second harmonic of cw Nd^{3+}:YAG laser (Verdi-10), was regeneratively amplified with 1 kHz repetition rate (Legend Elite USP) providing ≈100 fs pulses (FWHM) with energy ≈3 mJ pulse^{-1}. The output at 800 nm was split in two separate beams with ≈2 W and ≈1 W average power. The first beam was used for pumping an optical parametric amplifier (OPerA Solo) with pulse duration $\tau_P \approx 100$ fs (FWHM), tuning range 0.24–20 μm and pulse energies, E_P, up to ≈40 μJ. The second laser beam at 800 nm was converted to the second harmonic in a 1 mm BBO crystal for using as a pump source at 400 nm. One-photon induced fluorescence emission of **1** was observed perpendicular to the excitation beam (in order to easily separate spontaneous fluorescence photons from scattered stimulated emission and quenching photons) and the collected integrated fluorescence was measured with an Ocean Optics HR4000 spectrometer. The laser output of the OPerA Solo in the spectral range 600–1800 nm was delayed by ~10 ps relative to the 400 nm pump beam and used as a fluorescence quenching laser source with pulse duration ≈100 fs (FWHM). The nature of fluorescence quenching is based on one- or two-photon stimulated emission transitions in **1** that can dramatically depopulate the first excited electronic state S_1 and decrease the fluorescence intensity observed perpendicular to the excitation beam. The pump and quenching beams, with vertically oriented linear polarizations, were focused to a waist of radius ~0.4 mm (HW1/e^{2}M) for each beam, and recombined at a small angle ($<5^\circ$) within the sample solutions in a 1 mm path length quartz cuvette. In the case of one-photon quenching the degree of fluorescence quenching, $1 - I_F/I_{F0}$, (I_F and I_{F0} are the integral fluorescence intensity collected from one excitation pulse with and without the quenching beam, respectively) can be expressed by Equation (3):[17]

$$1 - I_F/I_{F0} = \frac{2\lambda_q \sigma_{10}(\lambda_q)}{\pi hc({}^{p}r_0^2 + {}^{q}r_0^2)} {}^{q}E_P \qquad (3)$$

where λ_q, $\sigma_{10}(\lambda_q)$, h, c, ${}^{p}r_0$, ${}^{q}r_0$ and ${}^{q}E_P$ are the quenching wavelength, one-photon stimulated emission cross section at λ_q, Planck's constant, velocity of light in vacuum, pump and quenching beam radius (HW1/e^{2}M), and pulse energy of the quenching beam, respectively. In the case of two-photon fluorescence quenching, Equation (3) can be written as Equation (4):[17]

$$1 - I_F/I_{F0} = (8/\pi^5)^{1/2} \frac{\lambda_q^2 \delta_{2PE}(\lambda_q)}{h^2 c^2 \tau_q {}^{q}r_0^2 (2{}^{p}r_0^2 + {}^{q}r_0^2)} {}^{q}E_P^2 \qquad (4)$$

where τ_q and $\delta_{2PE}(\lambda_q)$ are the quenching pulse duration (HW1/eM) and two-photon stimulated emission cross section, respectively. The values of $\sigma_{10}(\lambda_q)$ and $\delta_{2PE}(\lambda_q)$ can be obtained from the slopes of corresponding linear experimental dependences $1 - I_F/I_{F0} \sim \sigma_{10}(\lambda_q)^q E_P$ and $1 - I_F/I_{F0} \sim \delta_{2PE}(\lambda_q)^q E_P^2$. It should be mentioned that Equations (3) and (4) were obtained for Gaussian (in time and space) pumping and quenching beams taking into account some reasonable approximations described previously[17] that corresponded to the experimental conditions employed. All one- and two-photon stimulated transition measurements were performed in $CHCl_3$. The fluorescence quantum yield of **1** in $CHCl_3$ was independent of the excitation wavelength over a broad spectral range. This suggests no participation of direct radiationless transitions $S_n \rightarrow S_0$ (S_n is a highly excited electronic state). It means that the fluorescence intensity of **1** was not quenched by an excited-state absorption mechanism. No photochemical and other accumulative effects were observed in the samples under the prevailing experimental conditions. Also it should be mentioned that under femtosecond STED we should take into account the influence of possible 2PA processes from the high unrelaxed vibrational level of the ground state S_0. Therefore, linear dependences [Eqs. (3) and (4)] were observed for the small values of the degree of fluorescence quenching $1 - I_F/I_{F0}$.

Preparation of Dye-Encapsulated Micelles, Cell Incubation, and Fluorescence Bioimaging Methodologies: A solution of 5 mg dye in CH_2Cl_2 (5 mL) was mixed with Pluronic F 108NF (100 mg) in water (5 mL). The resulting mixture was stirred at room temperature for 48 h to slowly evaporate the CH_2Cl_2. The solution of micelles was then filtered through a 0.22 μm cut-off membrane filter for cell incubation. The final dye concentration was approximately 0.8 mM in water, as estimated by absorption spectra. An epithelial colorectal carcinoma cell line HCT 116, purchased from ATCC (America Type Culture Collection, Manassas, VA), was used. The cells were incubated in RPMI-1640 medium (Invitrogen, Carlsbad, CA, USA), supplemented with 10% fetal bovine serum (FBS), 100 units mL^{-1} penicillin–streptomycin, and incubated at 37 °C in a 95% humidified atmosphere containing 5% CO_2. HCT 116 cells were placed onto poly-D-lysine-coated coverslips inserted into 24-well glass plates (20000 cells per well) and incubated for 36 h before incubating with the fluorescent probes. A 0.8 mM stock solution of the fluorescent probe in Pluronic F 108 NF micelles was suspended in water. A diluted solution of probe (50 μM) by RPMI-1640 medium was then freshly prepared and placed over the cells for a 3 h period. After incubation, the cells were washed with PBS (3–5×) and fixed using 3.7% formaldehyde solution for 15 min at 37 °C. To reduce autofluorescence, a fresh solution of $NaBH_4$ (1 mg mL^{-1}) in PBS (pH 8.0), which was prepared by adding a few drops of 0.1 M NaOH solution into PBS (pH 7.2), was used for treating the fixed cells for 15 min (2×). The plates were washed twice with PBS, followed by water. Finally, the glass coverslips were mounted using Prolong Gold mounting medium for microscopy imaging. Conventional one-photon induced fluorescence microscopy (1PFM) images were obtained using inverted microscope (Olympus IX70) equipped with a QImaging cooled CCD (Model Retiga EXi) and excitation with a 100 W mercury lamp. 2PFM imaging was performed using a modified Olympus Fluoview FV300 microscope system coupled to a tunable Coherent Mira 900F Ti:sapphire (76 MHz, modelocked, femtosecond laser tuned to 940 nm). The two-photon induced fluorescence was collected with a 60× microscope objective (UPLANSAPO 60×, NA = 1.35, Olympus). An emission short-pass filter (cutoff 800 nm) was placed in the microscope scan head to avoid background irradiance from the excitation source. Consecutive layers, separated by approximately 0.15 μm, were recorded to create a 3D reconstruction from overlaid 2PFM images.

Acknowledgements

We acknowledge the National Institute of Biomedical Imaging and Bioengineering of the National Institutes of Health (1 R15 EB008858-01), the National Academy of Sciences of Ukraine (grant 1.4.1.B/153), and the National Science Foundation (ECCS-0925712, CHE-0840431, and CHE-0832622). Professors Eric W. Van Stryland and David J. Hagan are acknowledged for kindly providing access to a Clark-MXR CPA-2010 laser system.

Keywords: absorption · fluorescence · fluorene derivatives · laser scanning fluorescence microscopy · two-photon stimulated emission depletion

[1] W. Denk, J. H. Strickler, W. W. Webb, *Science* **1990**, *248*, 73–76.
[2] J. B. Ding, K. T. Takasaki, B. L. Sabatini, *Neuron* **2009**, *63*, 429–437.
[3] G. Moneron, S. W. Hell, *Opt. Express* **2009**, *17*, 14567–14573.
[4] E. Maçôas, G. Marcelo, S. Pinto, T. Cañeque, A. M. Cuadro, J. J. Vaquero, J. M. G. Martinho, *Chem. Commun.* **2011**, *47*, 7374–7376.
[5] S. Kawata, Y. Kawata, *Chem. Rev.* **2000**, *100*, 1777–1788.
[6] C. C. Corredor, Z. L. Huang, K. D. Belfield, A. R. Morales, M. V. Bondar, *Chem. Mater.* **2007**, *19*, 5165–5173.
[7] B. H. Cumpston, S. P. Ananthavel, S. Barlow, D. L. Dyer, J. E. Ehrlich, L. L. Erskine, A. A. Heikal, S. M. Kuebler, I. Y. S. Lee, D. McCord-Maughon, J. Q. Qin, H. Rockel, M. Rumi, X. L. Wu, S. R. Marder, J. W. Perry, *Nature* **1999**, *398*, 51–54.
[8] K. D. Belfield, X. B. Ren, E. W. Van Stryland, D. J. Hagan, V. Dubikovsky, E. J. Miesak, *J. Am. Chem. Soc.* **2000**, *122*, 1217–1218.
[9] M. Charlot, N. Izard, O. Mongin, D. Riehl, M. Blanchard-Desce, *Chem. Phys. Lett.* **2006**, *417*, 297–302.
[10] T. C. Lin, G. S. He, Q. D. Zheng, P. N. Prasad, *J. Mater. Chem.* **2006**, *16*, 2490–2498.
[11] D. E. Reisner, R. W. Field, J. L. Kinsey, H. L. Dai, *J. Chem. Phys.* **1984**, *80*, 5968–5978.
[12] A. Yassar, F. Garnier, H. Jaafari, N. Rebiere-Galy, M. Frigoli, C. Moustrou, A. Samat, R. Guglielmetti, *Appl. Phys. Lett.* **2002**, *80*, 4297–4299.
[13] S. Lattante, G. Barbarella, L. Favaretto, G. Gigli, R. Cingolani, M. Anni, *Appl. Phys. Lett.* **2006**, *89*, 051111.
[14] T. Kobayashi, J. B. Savatier, G. Jordan, W. J. Blau, Y. Suzuki, T. Kaino, *Appl. Phys. Lett.* **2004**, *85*, 185–187.
[15] D. J. Gauthier, Q. L. Wu, S. E. Morin, T. W. Mossberg, *Phys. Rev. Lett.* **1992**, *68*, 464–467.
[16] O. Pfister, W. J. Brown, M. D. Stenner, D. J. Gauthier, *Phys. Rev. Lett.* **2001**, *86*, 4512–4515.
[17] K. D. Belfield, M. V. Bondar, C. O. Yanez, F. E. Hernandez, O. V. Przhonska, *J. Phys. Chem. B* **2009**, *113*, 7101–7106.
[18] K. D. Belfield, M. V. Bondar, C. O. Yanez, F. E. Hernandez, O. V. Przhonska, *J. Mater. Chem.* **2009**, *19*, 7498–7502.
[19] M. Sheik-Bahae, A. A. Said, T. H. Wei, D. J. Hagan, E. W. Van Stryland, *IEEE J. Quantum Electron.* **1990**, *26*, 760–769.
[20] C. Xu, W. W. Webb, *J. Opt. Soc. Am. B* **1996**, *13*, 481–491.
[21] J. R. Lakowicz, I. Gryczynski, *Topics in Fluorescence Spectroscopy, Vol. 5: Nonlinear and Two-Photon-Induced Fluorescence*, Plenum Press, New York, **1997**.
[22] J. R. Lakowicz, I. Gryczynski, J. Kusba, V. Bogdanov, *Photochem. Photobiol.* **1994**, *60*, 546–562.
[23] J. Kuśba, J. R. Lakowicz, *J. Chem. Phys.* **1999**, *111*, 89–99.
[24] I. K. J. Gryczynski, Z. Gryczynski, H. Malak, J. R. Lakowicz, *J. Fluoresc.* **1998**, *8*, 253–261.
[25] I. Gryczynski, V. Bogdanov, J. R. Lakowicz, *J. Fluoresc.* **1993**, *3*, 85–92.
[26] V. Westphal, J. Seeger, T. Salditt, S. W. Hell, *J. Phys. B* **2005**, *38*, S695–S705.

[27] V. Westphal, S. O. Rizzoli, M. A. Lauterbach, D. Kamin, R. Jahn, S. W. Hell, *Science* **2008**, *320*, 246 – 249.
[28] S. W. Hell, J. Wichmann, *Opt. Lett.* **1994**, *19*, 780 – 782.
[29] T. A. Klar, S. Jakobs, M. Dyba, A. Egner, S. W. Hell, *Proc. Natl. Acad. Sci. USA* **2000**, *97*, 8206 – 8210.
[30] K. D. Belfield, M. V. Bondar, O. D. Kachkovsky, O. V. Przhonska, S. Yao, *J. Lumin.* **2007**, *126*, 14 – 20.
[31] J. R. Lakowicz, *Principles of Fluorescence Spectroscopy*, Kluwer, New York, **1999**.
[32] J. Galbán, E. Mateos, V. Cebolla, A. Domínguez, A. Delgado-Camón, S. de Marcos, I. Sanz-Vicente, V. Sanz, *Analyst* **2009**, *134*, 2286 – 2292.
[33] J. Tomasi, M. Persico, *Chem. Rev.* **1994**, *94*, 2027 – 2094.
[34] K. D. Belfield, M. V. Bondar, F. E. Hernandezt, O. V. Przhonska, S. Yao, *J. Phys. Chem. B* **2007**, *111*, 12723 – 12729.
[35] X. N. Wang, D. M. Nguyen, C. O. Yanez, L. Rodriguez, H.-Y. Ahn, M. V. Bondar, K. D. Belfield, *J. Am. Chem. Soc.* **2010**, *132*, 12237 – 12239.
[36] A. V. Deshpande, A. Beidoun, A. Penzkofer, G. Wagenblast, *Chem. Phys.* **1990**, *142*, 123 – 131.
[37] K. Ohta, L. Antonov, S. Yamada, K. Kamada, *J. Chem. Phys.* **2007**, *127*, 084504.
[38] S. Yao, H.-Y. Ahn, X. H. Wang, J. Fu, E. W. Van Stryland, D. J. Hagan, K. D. Belfield, *J. Org. Chem.* **2010**, *75*, 3965 – 3974.
[39] C. D. Andrade, C. O. Yanez, M. A. Qaddoura, X. Wang, C. L. Arnett, S. A. Coombs, R. Bassiouni, M. V. Bondar, K. D. Belfield, *J. Fluoresc.* **2011**, *21*, 1223 – 1230.
[40] K. H. Lee, Y. S. Kwon, L. K. Kang, G. Y. Kim, J. H. Seo, Y. K. Kim, S. S. Yoon, *Synth. Met.* **2009**, *159*, 2603 – 2608.
[41] A. R. Morales, K. J. Schafer-Hales, C. O. Yanez, M. V. Bondar, O. V. Przhonska, A. I. Marcus, K. D. Belfield, *ChemPhysChem* **2009**, *10*, 2073 – 2081.
[42] M. Mardelli, J. Olmsted, *J. Photochem.* **1977**, *7*, 277 – 285.
[43] C. C. Corredor, K. D. Belfield, M. V. Bondar, O. V. Przhonska, S. Yao, *J. Photochem. Photobiol. A* **2006**, *184*, 105 – 112.
[44] N. S. Makarov, M. Drobizhev, A. Rebane, *Opt. Express* **2008**, *16*, 4029 – 4047.
[45] J. Fu, L. A. Padilha, D. J. Hagan, E. W. Van Stryland, O. V. Przhonska, M. V. Bondar, Y. L. Slominsky, A. D. Kachkovski, *J. Opt. Soc. Am. B* **2007**, *24*, 67 – 76.
[46] L. A. Padilha, S. Webster, O. V. Przhonska, H. H. Hu, D. Peceli, J. L. Rosch, M. V. Bondar, A. O. Gerasov, Y. P. Kovtun, M. P. Shandura, A. D. Kachkovski, D. J. Hagan, E. W. Van Stryland, *J. Mater. Chem.* **2009**, *19*, 7503 – 7513.

Received: June 14, 2011
Published online on August 19, 2011

